Modeling and Driving Piezoelectric Resonant Blade Elements

Sam Ben-Yaakov* and Natan Krihely
Power Electronics Laboratory
Department of Electrical and Computer Engineering
Ben-Gurion University of the Negev
P.0.Box 653, Beer-Sheva 84105
ISRAEL
Tel: +972-8-6461561; Fax: +972-8-6472949;
Email: sby@ee.bgu.ac.il ; Website: http://www.ee.bgu.ac.il/~pel

***Abstract*— Piezoelectric Resonant Blade elements (PRB) are useful in applications such as light choppers, laser beam scanners, fans and others. Three methods are proposed for extracting the parameters of the PRB equivalent circuit model: two are direct methods and one is based on an iteration procedure that looks for the least square error. Drive needs for a PRB are discussed and possible drive alternatives are explored. The results of theoretical derivation for parameter extraction and drive requirements were verified against simulation and experiments.**

Keywords-Piezoelectric resonant blade; modeling; drivers; least square fitting.

I. INTRODUCTION

Piezoelectric Resonant Blade elements (PRB) can be used advantageously in a number of specialized applications such as light choppers, laser beam scanners, fans and others. The PRB belong to the general family of piezoelectric devices and in particular to the group that utilize the piezoelectric effect to generate motion such as motors and actuators [1]. The PRB are normally low power devices that have a resonant nature and therefore need to be driven at a specific frequency to optimize their performance. The objective of this work was to define the drive needs for PRB type devices. For this purpose we modeled the device, developed methods for extracting its model parameters and explored the possible drive alternatives for it.

II. THE PIEZOELECTRIC RESONANT BLADE (PRB) DEVICE MODEL

A typical PRB device (Fig. 1) is composed of a bimorphs piezoelectric element that is bonded to a van and to a mounting base. When excited at the proper frequency the bimorphs element will bend the van attached to it and the whole structure will vibrate. Optimum operation is obtained when the drive frequency equals the mechanical resonant frequency of the structure. From the electrical point of view the admittance measured at the PRB electrical terminals looks as a multiresonant network (Fig. 2). As can be observed in Fig. 2, the Q (quality factor) at the fundamental resonance frequency

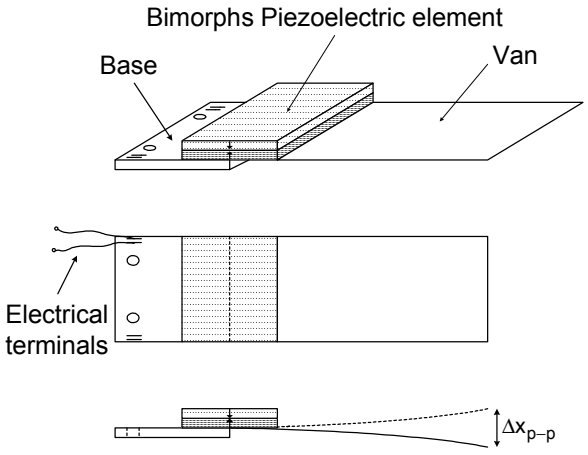

Figure 1. The piezoelectric resonant blade element.

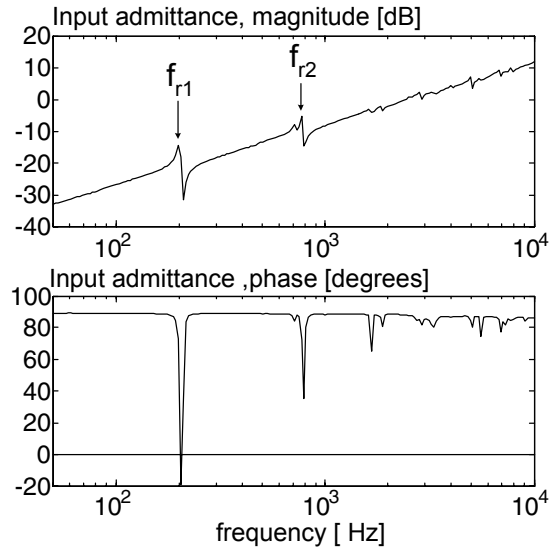

Figure 2. Input admittance of the PRB element. The series resonant frequencies f_{r1}, f_{r2} correspond to first and second vibration modes.

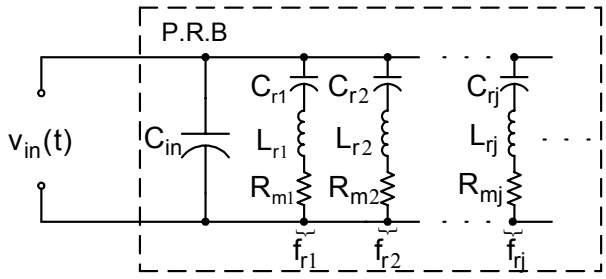

Figure 3. Equivalent circuit model of the PRB element. C_{in} is the dielectric capacitance of the input electrodes.

f_{r1} is higher than at f_{r2}, which implies that f_{r1} is a better choice for maximum power transfer [2]. Each resonant frequency corresponds to a specific resonant vibration mode of the device. This fact is used in the simplest lump model of the PRB that includes a number series resonant networks connecting in parallel (Fig. 3). The dielectric capacitance of the input electrodes C_{in} in this model is, in fact, the only truly electrical element while all the other reactive and passive elements emulate the mechanical parameters of the PRB and the power delivered by it to losses and actual mechanical work. At around the optimal frequency (the first resonance mode in present case), the PRB model can be reduced to a simpler lump model (Fig. 4) in which the total input capacitance C is equal to the dielectric capacitance C_{in} plus the residual capacitance (ΔC) due to higher resonant frequencies:

$$C = C_{in} + \Delta C = C_{in} + \sum_{i=2}^{\infty} C_{ri} \,. \qquad (1)$$

The input admittance of the PRB (Fig. 4) will thus be:

$$Y_{in}(j\omega) = j\omega C + \frac{1}{R_m + j\omega L_r + 1/j\omega C_r} \qquad (2)$$

where C, R_m, C_r, L_r refer to the values at around the resonance frequency of interest (the first one in present case).

III. Model Parameters Extraction

Considering first the extraction of C by a measurement. It becomes clear from the examination of the input admittance of the PRB (Fig. 5), that one should be careful in selecting the operating frequency of a capacitance meter, if such an instrument is used to measure C. If the capacitance measurements are made below f_{r1}, then it comprises of C_{in} plus all the C_r capacitors, including C_{r1}. The correct value of C can be estimated by measuring the admittance at a frequency $Y_{in}(f_C)$ above the resonant frequency of interest, f_{r1} in present case, but below the second resonant frequency.

Referring to Fig. 5, C can be obtained from:

$$Y_{in}(f_C) \approx 20\log(2\pi f_C C) \,. \qquad (3)$$

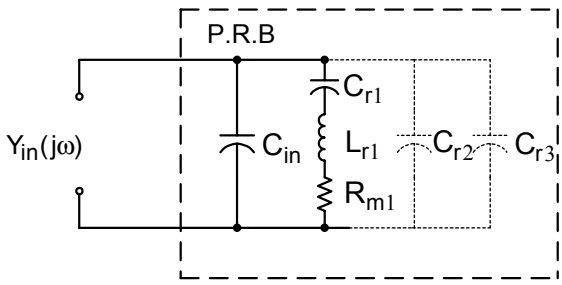

Figure 4. Approximate electrical circuit model near the first resonant frequency. Dashed branches corresponding to the strong capacitive influence of higher resonance harmonics.

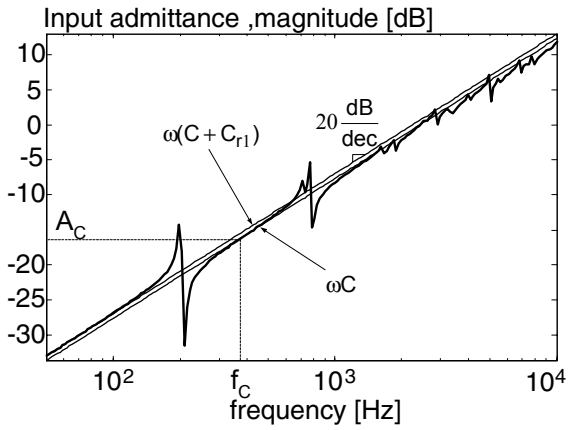

Figure 5. Input admittance and its asymptotes.

Another possibility for extracting C would be to measure the admittance at the resonant frequency of interest. From (2):

$$Y_{in}(f_r) = \frac{1}{R_m} + j2\pi f_r C \qquad (4)$$

and hence

$$C \approx \frac{\mathrm{Im}[Y_{in}(f_r)]}{2\pi f_r} \,. \qquad (5)$$

The series resonant frequency f_r is recognized by looking for the frequency at which $\mathrm{Re}[Y_{in}(f)]$ reaches the maximum value [3] .

An additional method for extracting C is by fitting the measurement data to all of the model parameters as detailed below.

A number of methods were proposed earlier for extracting the R_m, C_r and L_r parameters [2, 4]. Some rely on the fact that the studied element has a high quality factor (Q) and consequently the phase shifts of the admittance are large and passing through the values of $\pm 45^0$. In the case of a PRB, the Q factor may not be high especially when the device is driven by a high voltage signal that may cause the PRB to enter a

stiffness non-linear region due to the large deflection (Fig. 6). Consequently there is a need to apply here a parameter extraction method that could be used even for low Q cases. In this study we explored several such methods. To this end we first generated equivalent circuits for the various frequency ranges around the resonant frequency (Fig. 7). Next we derived the relationships between the original parameters and the values of the equivalent circuit elements. Based on these relationships we developed three methods for extracting the parameters of the lumped PRB model. The first two methods assume that C is known (measured independently) while the third one without an apriori knowledge of C.

A. Method A - C is known. Frequency range $f < f_r$.

In this method we translate Fig. 4 at $f < f_r$ to the sequence of the equivalent circuits shown in Fig. 7 (a), (b) and (c). By working from Fig. 7c backward to Fig. 7a and applying the relationships between the measured admittance $Y_{in}(f)$ and the elements in the subcircuits, the following equations are obtained (the subscript (i) represent values for a specific frequency f_i):

$$R_{eqi} = \frac{1}{\mathrm{Re}\{Y_{in}(f_i)\}} \tag{6}$$

$$C_{eqi} = \frac{\mathrm{Im}\{Y_{in}(f_i)\}}{\omega_i} \tag{7}$$

$$C_{pi} = C_{eqi} - C \tag{8}$$

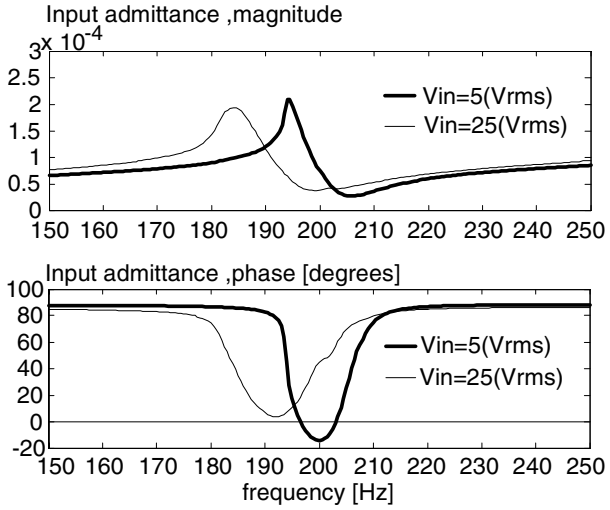

Figure 6. Input admittance of experimental PRB for two excitation voltages.

$$C_{si} = \frac{1 + (\omega_i C_{pi} R_{eqi})^2}{\omega_i^2 C_{pi} R_{eqi}^2} \tag{9}$$

$$C_{si} = \frac{C_r}{1 - \omega_i^2 L_r C_r}. \tag{10}$$

Equations (6)-(9) show how C_{si} can be derived from the admittance $Y_{in}(f_i)$ measurements. Equation (10) includes two unknowns: L_r and C_r. These can be calculated by taking two measurements at two frequencies f_1 and f_2 to obtain C_{s1} and C_{s2}:

$$C_{s1} = \frac{C_r}{1 - \omega_1^2 L_r C_r} \tag{11}$$

$$C_{s2} = \frac{C_r}{1 - \omega_2^2 L_r C_r}. \tag{12}$$

Solving (11) and (12) for L_r and C_r, one obtains:

$$L_r = \frac{C_{s1} - C_{s2}}{C_{s1} C_{s2} (\omega_1^2 - \omega_2^2)} \tag{13}$$

$$C_r = \frac{C_{sj}}{(1 + \omega_j^2 C_{sj} L_r)}. \tag{14}$$

The index "j" in (14) means that C_r can be calculated either from sample 1 or 2.

Similarly, R_m can be estimated from either sample:

$$R_m = \frac{R_{eqj}}{1 + (\omega_j C_{pj} R_{eqj})^2}. \tag{15}$$

B. Method B - C is known. Frequency range $f > f_r$.

In this method we translate Fig. 4 at $f > f_r$ to the sequence of the equivalent circuits shown in Fig. 7 (d), (e) and (f). Then, by the same procedure as method A, one can calculate R_m, C_r, L_r by the following equations:

$$L_{pi} = \frac{1}{(C - C_{eqi})\omega_i^2} \tag{16}$$

$$L_{si} = \frac{R_{eqi}^2 L_{pi}}{R_{eqi}^2 + (\omega_i L_{pi})^2} \tag{17}$$

where C_{eqi} and R_{eqi} are obtained from (7) and (6) respectively.

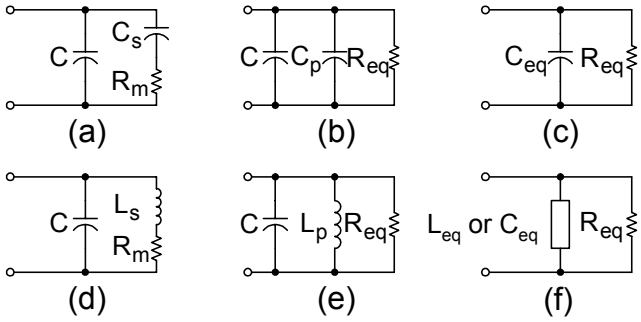

Figure 7. Equivalent circuits of the PRB at various operating frequency ranges. (a), (b), (c) are equivalent circuits for $f < f_r$; (d), (e), (f) are equivalent circuits for $f > f_r$. In last frequency range the input admittance could be capacitive or inductive.

$$L_{si} = L_r - \frac{1}{\omega_i^2 C_r} \tag{18}$$

$$L_{s1} = L_r - \frac{1}{\omega_1^2 C_r} \tag{19}$$

$$L_{s2} = L_r - \frac{1}{\omega_2^2 C_r}. \tag{20}$$

Applying (19) and (20) the expressions for the series induction and capacitance are derived as:

$$C_r = \left(\frac{1}{\omega_2^2} - \frac{1}{\omega_1^2}\right)\frac{1}{(L_{s1} - L_{s2})} \tag{21}$$

$$L_r = L_{sj} + \frac{1}{\omega_j^2 C_r} \tag{22}$$

and

$$R_m = \frac{R_{eqj}}{1 + (\omega_j C_{pj} R_{eqj})^2}. \tag{23}$$

Methods A and B are thus based on the selection of two admittance measurements at two different frequencies. These are then used to calculate R_m, C_r and L_r around the frequency range of interest $f < f_r$ (method A) or $f > f_r$ (method B). However, since the selection of the two admittance points is done manually, there is no guarantee that the selected points will indeed yield the best fit over the desired range. The least square fitting method (Method C) described below overcomes this obstacle by searching automatically for the pair of admittance points that will produce the best fit over the given range.

C. Method C - C is unknown

This method is similar to the previous ones except that an iteration process is used to select C that minimizes the error between the model and measured admittance. This was implemented by MATLAB program that follows the flowchart of Fig. 8.

Referring to Fig. 8, a sequence of admittance measurements are taken and represented by a vector Y at the start of the calculation according to the proposed method. The notation Y[i] means: the (i)th component of the vector Y. By guessing some initial C and selecting two admittance points (m) and (n), Y is estimated by either method A or B over the vector range from $i_{initial}$ to i_{final}. The function g(f[m], f[n]) calculates the input admittance (represented by Y_{calc}) from any two points m and n, and the least square difference between the estimated admittance and the measured one Y is calculated over the chosen range ($i_{initial}$ to i_{final}). This process repeats until all C and measured admittance values have been scanned over the predetermined ranges, and the best fit is detected. The set of values for C, L_r, C_r, R_m that produced the minimum error between Y to Y_{calc} are finally selected as the optimal solution.

IV. DRIVING THE PRB

Since the PRB's resonant frequency reflects its mechanical vibration resonance, which depends on mass and stiffness, the PRB is normally a low frequency device (the resonance frequency of the PRB under investigation was about 200Hz). Consequently, drive methods that are appropriate for high frequency piezoelectric transformers (PZT) [5] may not apply here. In particular, previously described techniques for that achieve Zero Voltage Switching (ZVS) by placing an inductor in series with the PRB or operating it at a frequency that the PZT looks inductive [6], are not practical for the PRB. This is because the inductance (L_{series}) that needs to be placed in series with the PRB to achieve ZVS,

$$L_{series} > \frac{1}{(2\pi f_r)^2 C} \tag{24}$$

is very large. For the PRB used in this study, L_{series}>10H which is of course impractical.

Operating the PRB above the series resonant frequency, when it looks inductive, is also impractical. This is because the PRB is a relatively low Q element and hence the stored energy is insufficient to charge the parasitic capacitors [6]. Furthermore, operation off resonance is undesirable since the PRB's energy transfer is poor when the drive frequency deviates from the series resonant frequency. Experiments conducted during this study showed that driving the PRB via a small inductor is undesirable since it produces oscillations at high frequency that disturb the PRB vibrations.

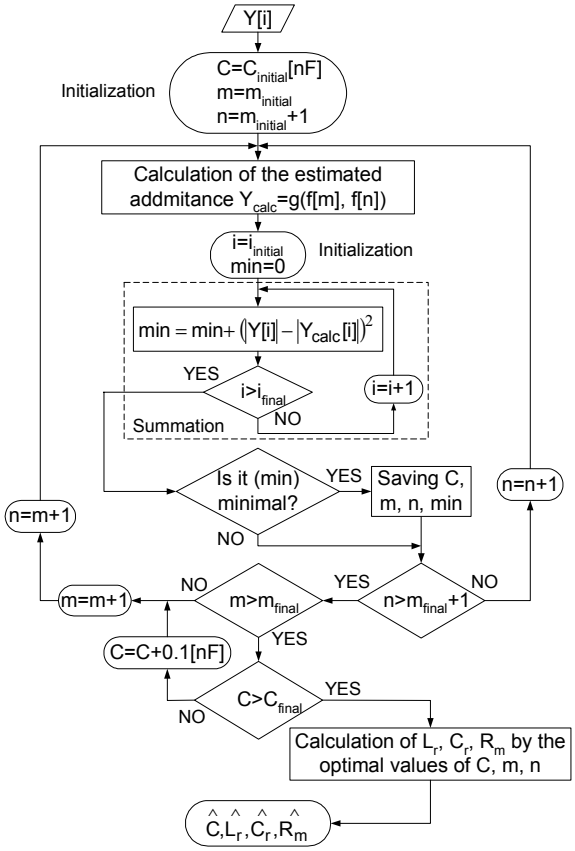

Figure 8. MATLAB least square fitting algorithm.

In this study we considered three practical PRB drive alternatives: a sinusoidal waveform, a squarewave, and a trapezoid waveform. The pros and cons are as follows:

Sinusoidal. Pros: Low EMI, no harmonics that might excite undesired vibrations. Cons: Difficult to generate, low efficiency, input current phase is displaced due to C. Consequently, the phase of the input current can not be used as an indicator for the resonance frequency of the PRB. This complicates the design of an auto tracking circuitry based on the Phase Lock Loop (PLL) approach [7].

Squarewave. Pros: Simple to generate, simplifies PLL operation. Cons: High EMI, rich in harmonics that might excite undesired vibrations.

Trapezoidal. Pros: Relatively low EMI, low in harmonics that might excite undesired vibrations, relatively easy to generate, simplifies PLL operation. Cons: Somewhat more difficult to generate than a squarewave.

V. EXPERIMENTAL RESULTS

A PRB RBL1-006 model (Piezo Systems, Inc, USA) was measured, modeled, simulated and driven. The manufacture's parameters of the device are: input voltage (to inverter) 44Vdc, current 7.5mA, power consumption 300mW, nominal resonant frequency 185Hz, tip amplitude (ΔX_{p-p}) 0.29inches, weight 3.8grams, temperature range -40° C to 70° C.

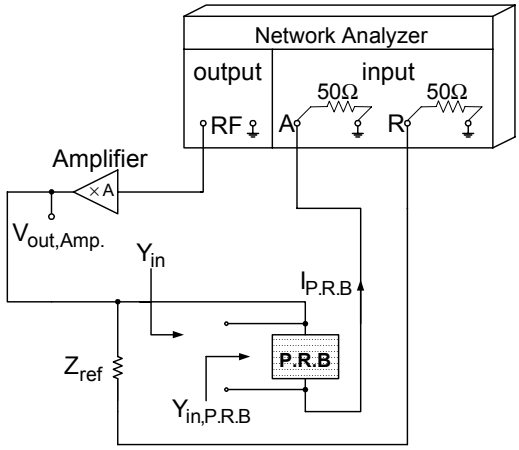

Figure 9. Network analyzer measurements setup.

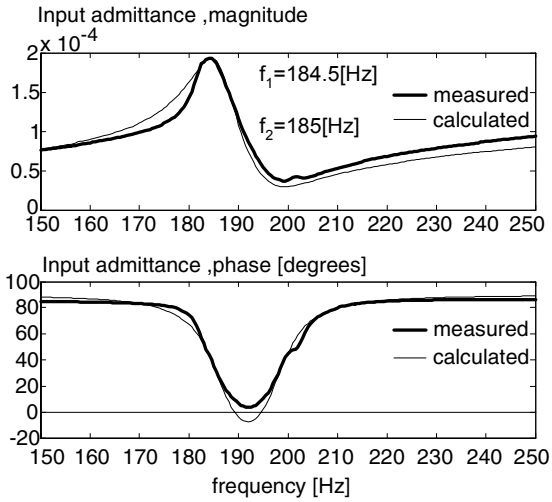

Figure 10. Comparison between measured and model calculated admittances. Model parameters extraction by Method C. Fitting range: 181Hz to 189Hz ($f < f_r$). f_1 and f_2 were found by the MATLAB least square fitting algorithm as to provide the best fit. Estimated parameters: C=60.7nF, L_r=95.481H, C_r=7.6458nF, R_m=5987.6Ω, f_r=186.27Hz.

A network analyzer model HP4395A was applied (Fig. 9) for measuring the input admittance. The measurement data was corrected by subtracting the series resistance of 50 Ohm (Fig. 9) to obtain the admittance of the PRB. Typical measurements are shown in Figs. 2, 5 and 6. By applying the model parameters extraction method developed in this study, it was possible to get a very good fit over a small frequency range (e.g. Figs. 10, 11).

The fitting is deemed to be excellent, considering the fact that the parameters of the PRB are expected to change over the fitted frequency range. In particular, as the frequency is getting closer to the series resonant, the amplitude of the vibration increase and the average stiffness may change and consequently the parameters of the model will vary. Furthermore R_m, which emulates internal friction losses and mechanical work, is also expected to vary as the amplitude of the vibration changes. Best fitting results were obtained by the proposed iterative least-square fitting algorithm (Method C) which estimates R_m, C_r, L_r and C (Figs. 10, 11). Measuring C

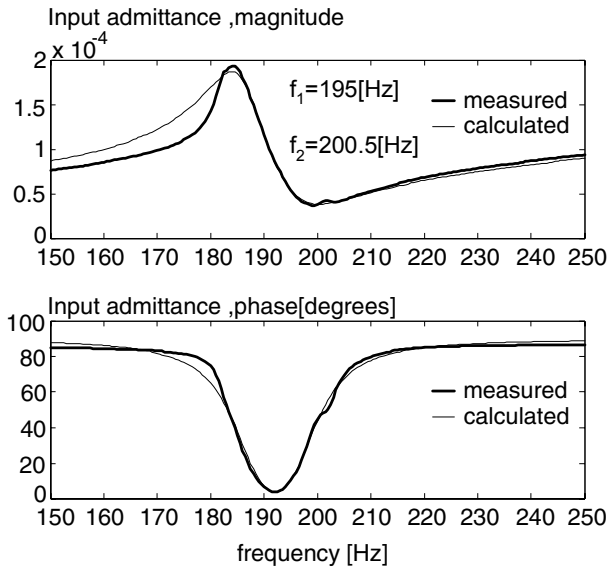

Figure 11. Comparison between measured and model calculated admittances. Model parameters extraction by Method C. Fitting range: 187.5Hz to 204.5Hz ($f > f_r$). Estimated parameters: C=67.8nF, L_r=84.551H, C_r=8.6184nF, R_m=6508Ω, f_r=186.443Hz.

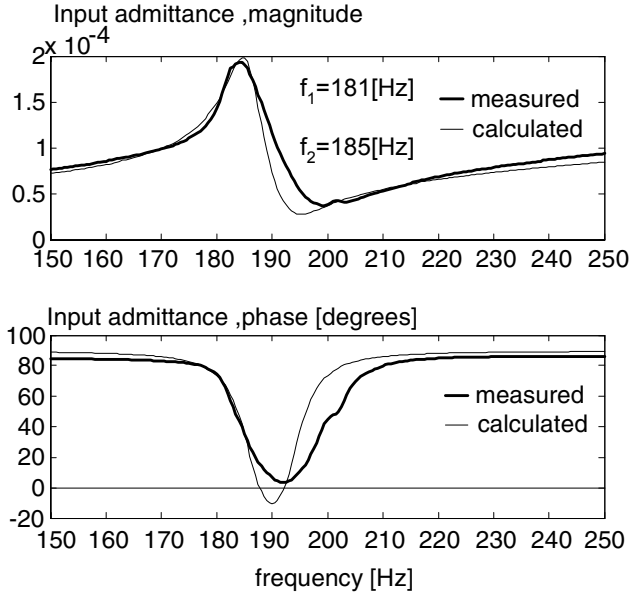

Figure 12. Comparison between measured and model calculated admittances. Model parameters extraction by Method A; C was calculated by eq. (3). f_1 and f_2 are two arbitrary frequencies in the range $f<f_r$. Estimated parameters: C=59.961nF, L_r=134.8H, C_r=5.4363nF, R_m=5773Ω, f_r=185.92Hz.

independently and using its value in the estimate of R_m, C_r, L_r (Method A) produced an inferior fit (Fig. 12) as compared to Method C.

The various drive alternatives were examined experimentally by driving the PRB with a sine wave, squarewave and trapezoid signal (Fig. 13). The results confirm the general consideration discussion in Section IV.

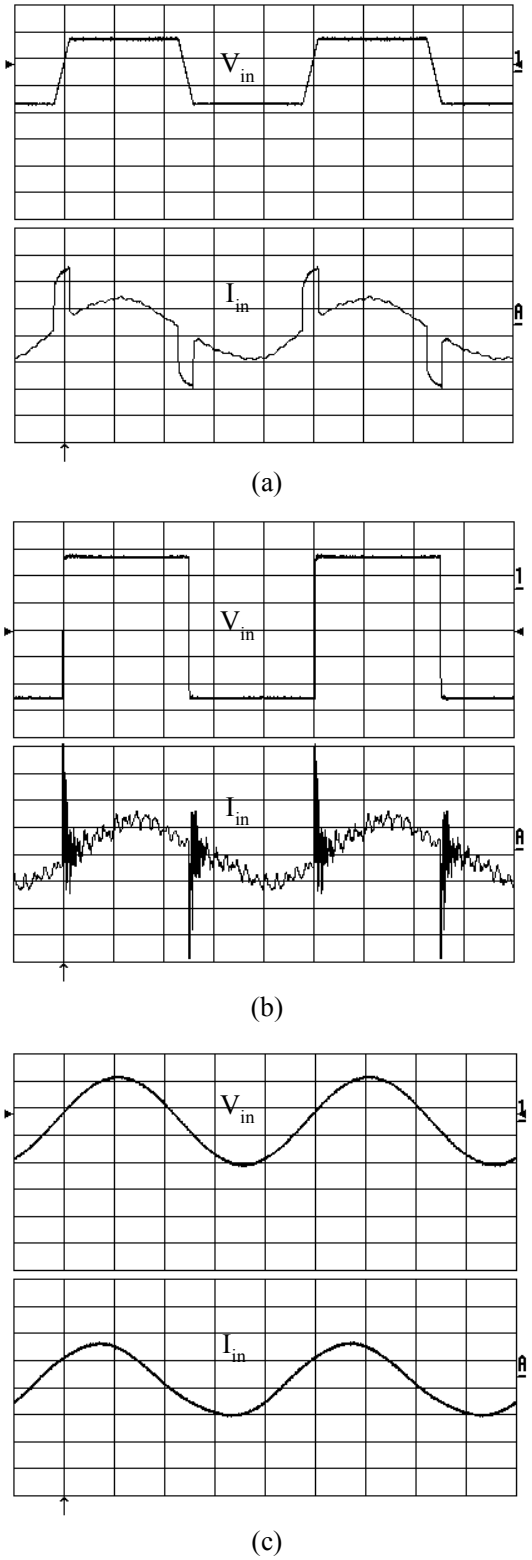

Figure 13. Experimental drive waveforms. (a) Trapezoid wave drive (2V/div., 0.5mA/div.), (b) Squarewave drive (2V/div., 1mA/div.), (c) Sine wave drive (2V/div., 0.5mA/div.).

VI. Discussion and Conclusions

This investigation explored the modeling and drive aspects of PRB devices. The proposed model extraction methods overcome the difficulties of previous methods that assume a high Q element. The model extraction methods explored here is shown to be accurate, to within the physical limitation resulting from the fact that the PRB is a non-linear device. That is, considering the fact that from the theoretical point of view a linear network cannot model it over a large frequency range. The extracted model should thus be considered as an approximation or as an experimental fitting. Nonetheless, the model, as is, can be useful in the study of PRB drivers in open and closed loop configurations.

Among the three drive-waveform considered in this study, the trapezoidal waveform seems to be the optimal one. It is less likely to excite higher resonant frequencies, it has low EMI emission and is relatively easy to generate (applying a current limited source) as compared to the sinusoidal drive. An important feature of the trapezoidal drive is the fact that the input-current disturbances due to input capacitance C, last only during the ramp times. If this disturbance is blocked out, the current waveform is found to be in phase with the input voltage when the PRB is driven at its mechanical resonance. This could be useful in the designed of self locking driver.

Acknowledgment

This research was supported by THE ISRAEL SCIENCE FOUNDATION grant # 113/02-1.

References

[1] K. Uchino, *Piezoelectric actuators and ultrasonic motors*, Boston, MA: Kluwer Academic Publishers, 1996.

[2] V. Ferrari, D. Marioli, A. Taroni, "Theory, modeling and characterization of PZT-on-alumina resonant piezo-layers as acoustic-wave mass sensors", *Sensors and Actuators*, 2001, pp. 182-190.

[3] C. Y. Lin and F. C. Lee, "Design of a piezoelectric transformer converter and its matching networks", *IEEE Power Electronics Specialists Conf.*, 1994, pp. 607-612.

[4] S. Sherrit, H. D. Wiederick, B. K. Mukherjee, "Accurate equivalent circuits for unloaded piezoelectric resonators", *IEEE Ultrasonics Symposium Proceedings*, 1997, pp. 931-935.

[5] M. Sanz, P. Alou, R. Prieto, J. A. Cobos and J. Uceda "Comparison of different alternatives to drive piezoelectric transformers", *IEEE Applied Power Electronics Conf.*, 2002, pp. 358-364.

[6] S. Bronstein and S. Ben-Yaakov "Design considerations for achieving ZVS in a half bridge inverter that drives a piezoelectric transformer with no series inductor", *IEEE Power Electronics Specialists Conf.*, 2002, pp. 585-590.

[7] E. Dallago, A. Danioni, M. Passoni and G. Venchi, "Modelling of DC-DC converter based on a piezoelectric transformer and its control loop", *IEEE Power Electronics Specialists Conf.*, 2002, pp. 927-931.